

Flexible hybrid graphene-based NFC tag antenna for temperature monitoring application

Najwa Mohd Faudzi¹, Ahmad Rashidy Razali¹, Asrulnizam Abd Manaf², Nurul Huda Abd Rahman³, Ahmad Azlan Ab Aziz⁴, Syed Muhammad Hafiz⁵, Suraya Sulaiman⁵, Nora'zah Abdul Rashid⁵, Amirudin Ibrahim¹, Aiza Mahyuni Mozi¹

¹Centre for Electrical Engineering Studies, Universiti Teknologi MARA, Cawangan Pulau Pinang, Permatang Pauh Campus, Pulau Pinang, Malaysia

²Collaborative Microelectronic Design Excellence Center, Universiti Sains Malaysia, Pulau Pinang, Malaysia

³School of Electrical Engineering, College of Engineering, Universiti Teknologi MARA, Selangor, Malaysia

⁴Faculty of Engineering, Universiti Teknologi Brunei, Brunei Darussalam

⁵MIMOS Berhad, Kuala Lumpur, Malaysia

Article Info

Article history:

Received Jul 26, 2024

Revised Oct 17, 2024

Accepted Oct 30, 2024

Keywords:

Antenna

Graphene-based

Hybrid

Near field communication

Tag

Temperature monitoring

ABSTRACT

A hybrid graphene-based material, composed of reduced graphene oxide (rGO) and silver nanoparticle (AgNP), has been proposed for a near field communication (NFC) tag antenna with an integrated, flexible temperature monitoring circuit. The limited availability of high-conductivity graphene-based materials in the market has restricted the use of graphene in NFC tag applications. Therefore, this paper proposes a hybrid graphene-based composition featuring a high conductivity of 3.95×10^6 S/m. The feasibility of this material for NFC tags had not been validated previously, which is the main motivation for this research. The synthesis of the materials, along with the design, fabrication, and characterization of the NFC tag, is also presented. Results show that the inkjet-printed tag achieves a good reading range of up to 3 cm and demonstrates robustness against bending from 60° to 190° , maintaining a maximum reading range of 1.3 cm. Performance on various materials, such as plastic, paper, and carton, also shows minimal impact on frequency shifting. Additionally, the graphene-based NFC tag integrates well with the temperature circuit, effectively monitoring temperatures in the 20-60 °C range in real-time. This makes the developed tag suitable for applications such as food safety monitoring systems through NFC-integrated packaging.

This is an open access article under the [CC BY-SA](https://creativecommons.org/licenses/by-sa/4.0/) license.



Corresponding Author:

Ahmad Rashidy Razali

Centre for Electrical Engineering Studies, Universiti Teknologi MARA, Cawangan Pulau Pinang

Permatang Pauh Campus, 13500 Pulau Pinang, Malaysia

Email: ahmad073@uitm.edu.my

1. INTRODUCTION

Wireless communication is essential for sensing technology due to its flexibility in facilitating seamless data exchange, enabling real-time monitoring, and enhancing the adaptability of devices across diverse applications. One of the most popular wireless communications systems is the radio frequency identification (RFID) technology, which is widely used in many sensing applications, including health monitoring, food safety monitoring, temperature as well as humidity monitoring [1]-[3]. RFID can operate in different frequency ranges, which are low frequency (LF), high frequency (HF) and ultra-high frequency (UHF). Among all the available RFID technologies, HF as known as near field communication (NFC) system has attracted great attention due to its capability of communicating in a short distance of less than 10 cm,

which shows high security, as well as a simple operation process, which can be achieved only by using a smartphone as a reader [4].

The working principle of the NFC system involves inductive coupling between the reader and the tag in the near field region at a frequency of 13.56 MHz [5]. The NFC tag can receive energy from the reader to activate the NFC chip and any integrated electronic components, such as microcontrollers and sensors, without requiring an external power source like batteries. The primary element of the NFC system is the antenna, which is utilized for transmitting and receiving radio frequency signals. The antenna comprises a conductive coil element, a substrate, and a chip. The conducting element of an antenna is often comprised of a metal-based material, such as copper or aluminium [6], [7]. While these materials exhibit excellent electrical conductivity and mechanical properties, they have some limitations, such as being easily oxidized at ambient temperatures and cracked upon bending [8]. Consequently, the electrical conductivity can be greatly reduced upon oxidation, thus shortening the application life span. Other metal-based materials like silver nanoparticles (AgNPs) are also widely used as conductive material for antenna, as presented in [9], [10] due to their high electrical conductivity and oxidation resistance. However, the mass production and raw materials cost are way too high for AgNPs compared to copper and aluminium, making it less suitable for low-cost applications [11].

To address these constraints, carbon-based materials have emerged as a possible alternative to metal-based conductive materials for antennas due to their low cost, oxidation resistance, chemical stability, and mechanical flexibility [12]. The unusual features of carbon-based materials, particularly graphene, have attracted the interest of researchers. Graphene is a single sheet of graphite having a two-dimensional (2D) array of sp²-connected carbon atoms organized in a honeycomb hexagonal lattice structure. The characteristics of graphene include high electron mobility, light weight, flexibility, and biocompatibility [13], [14]. Previously, the research on graphene-based antenna was primarily aimed at the terahertz band [15], [16], but in 2015, some research on the graphene-based antenna for much lower frequency, HF and UHF, started to emerge [17]-[19]. However, the conductivity values of the graphene-based conductive materials, as proposed by other researchers [20], [21] are mostly two to three orders lower than the metal-based conductive materials, which are in the range of $\sim 10^4$ to $\sim 10^5$ S/m. This much lower conductivity compared to metal-based material will increase the antenna resistance, hence reducing the antenna efficiency. A few methods have been employed to improve the conductivity of the graphene-based materials, such as using binders like ethyl cellulose (EC) to prepare graphene ink [22]. However, this method is incompatible with heat-sensitive substrates like papers, PET, and textiles, as it requires high-temperature thermal annealing of up to 300 °C. Other methods suitable for low temperature resistance substrates include graphene layer stacking [20] and rolling compression [23], [24] techniques. However, achieving uniform compression and stacking poses challenges, as excessive compression and irregular stacking may lead to degradation of conductivity and graphene performance. One of the most promising methods for increasing conductivity is incorporating metallic nanoparticles with graphene [13], as it is compatible with a wide range of substrates and mechanically more stable. However, careful material selection and processing techniques must be considered to avoid external resistance. Previously, hybrid graphene-based materials have mainly been applied in flexible electronics and sensors [13], [24], [25], and to date, no HF antenna application has been demonstrated based on hybrid graphene-based materials.

Therefore, this paper proposes a new high-conductivity material composed of a hybrid composition of reduced graphene oxide (rGO) and AgNPs, intended for use as a conductive element in an NFC tag antenna and a flexible temperature monitoring circuit. The characterization of the hybrid graphene-based material and the design process of the NFC tag antenna are detailed in the methodology section. The validation process of the proposed material in NFC tag application is presented in the results and discussion section, where the simulation and experimental results of the NFC tag antenna are analyzed, focusing on its electrical properties and robustness, including bending and surface material sensitivity. Additionally, this section covers the embedded temperature sensor circuit and the enhancement of the NFC temperature monitoring app. The final section provides a summary of the paper and recommendations for future work.

2. MATERIALS AND METHODS

This section describes the characterization of hybrid graphene-based conductive ink, the design of NFC tag antenna and the fabrication process of the graphene-based NFC tag antenna.

2.1. Synthesis and characterization of hybrid graphene-based conductive ink

The hybrid graphene-based conductive ink was formulated through a chemical reduction method involving a combination of rGO and AgNPs, as explained in [26]. rGO is produced by applying further reductive exfoliation treatment to graphene oxide (GO) from Graphenea, USA, which was utilized as the

precursor for synthesizing graphene. By having fewer oxygen functional groups, rGO produces greater electrical conductivity and carrier mobility compared to GO [27]. A solution consisting of 50% rGO and 50% silver nitrate (AgNO₃), along with a reducing and encapsulating agent, was prepared and then incubated to facilitate the formation of AgNPs/rGO. Subsequently, the resulting black composite, collected post-centrifugation, was crushed, and deionized water was introduced to create the hybrid graphene-based colloid. The colloid was then converted into inkjet printable ink with a proprietary water-based formulation which are called Mi-GraphPrInk (MIMOS Berhad, Malaysia) with <10% solid content, pH ~6.8 and viscosity of ~2.39 cP.

The samples' structural characteristics were evaluated utilizing a scanning electron microscope (SEM) and transmission electron microscope (TEM). As illustrated in Figure 1, the TEM micrographs verify the configuration of AgNPs on rGO nanosheets. It is evident from Figure 1(a) that an abundance of AgNPs in spherical shape were deposited on the surface and at the border of the rGO. The AgNPs exhibit a particle size distribution ranging from 10 to 25 nanometers (Figure 1(b)). The lattice fringe spacing, as determined through measurement, is 0.24 nanometers (Figure 1(c)), which corresponds to the FCC lattice of the crystal plane (111) [26]. Figure 1(d) depicts the SEM image of the printed pattern, revealing a smooth and defect-free microstructure that facilitates electron movement. From the SEM image, the presence of AgNPs on the rGO nanosheets is confirmed. A good attachment between graphene and silver particles may contribute to the high conductivity of the material.

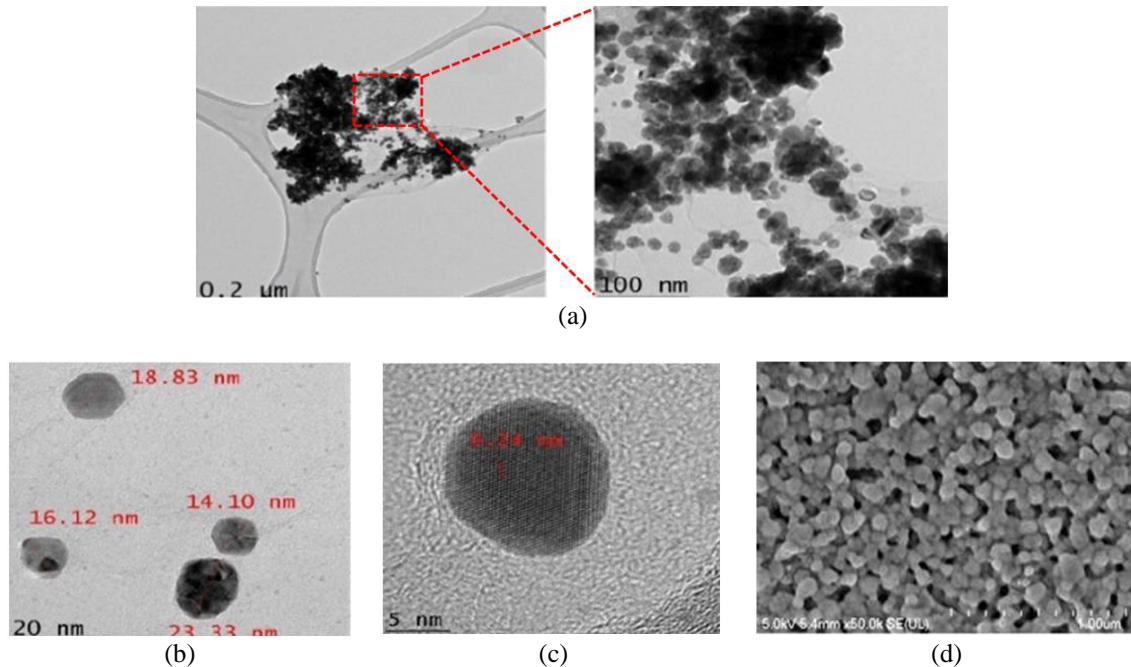


Figure 1. TEM images of (a) AgNP/rGO nanocomposites, (b) particle size distributions of AgNPs, (c) particle size distributions of AgNPs, and (d) SEM image of AgNP/rGO nanocomposites

The conductivity measurement of the hybrid-graphene-based ink, shown in Figure 2, was performed using the 4-Point Probe Loresta GX MCP-T700 from Mitsubishi Chemical Analytech Co. Ltd., as illustrated in Figure 2 (a). Four graphene square samples, each measuring 1×1 cm and with a thickness, *t* of 1 μm, were printed on the flexible PET substrate and measured using the 4-Point probe as shown in Figure 2(b). The resistance, *R* for each square was measured four times and the conductivity, σ value was then calculated using (1) until (3), where ρ_v , ρ_s and RCF indicates volume resistivity, surface resistivity and resistivity correction factor, respectively. The value for RCF used in this calculation is a constant value of 3.891 [28].

$$\sigma = \frac{1}{\rho_v} \tag{1}$$

$$\rho_v = R \cdot RCF \cdot t \tag{2}$$

$$\rho_s = R \cdot RCF = \rho_v \cdot \frac{1}{t} \tag{3}$$

The distribution of the conductivity values for each of the samples is illustrated in Figure 2(c). From the box plot, it can be seen that sample 1, 2, and 4 show a positively skewed distribution of the conductivity; meanwhile, only sample 3 shows a negatively skewed distribution. This trend indicates that the collected data is reliable and consistent, and some unavoidable human error during measurement might contribute to the high dispersion of the data set in sample 3. The mean conductivity value achieved from all the collected data and samples is 3.95×10^6 S/m. Therefore, this conductivity value is used for NFC tag antenna design in the subsequent section.

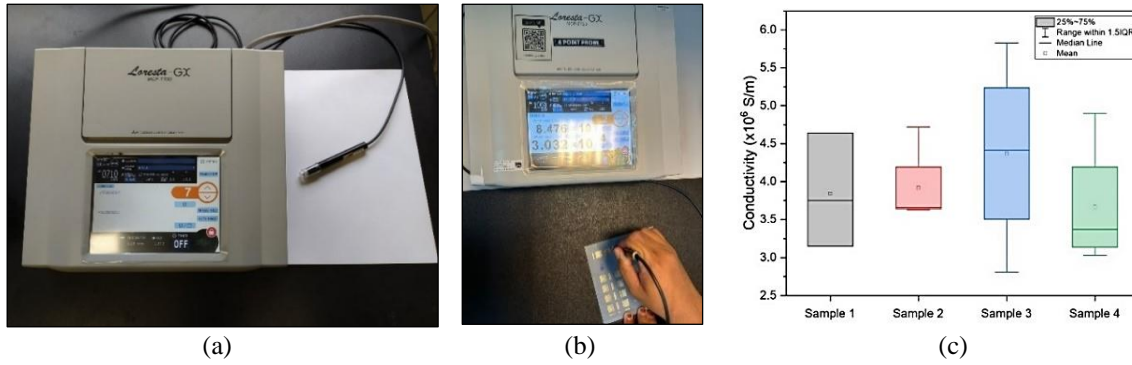


Figure 2. Conductivity measurement: (a) using 4-Point Probe Loresta GX MCP-T700, (b) measurement conducted on graphene samples, and (c) distribution of conductivity values for 4 samples

2.2. NFC tag antenna design

The NFC tag antenna in Figure 3 comprises an RLC resonance circuit, as illustrated in the simplified equivalent circuit model in Figure 3(a). The DC antenna resistance, R_a , indicates the loss of the antenna coil, which is specified by the width (w) and the length of the antenna coil. Meanwhile, the antenna inductance, L_a , depends on the geometrical parameters of the coil antenna, including the antenna length (a), width (b), number of turns (n), conductor's width (w), and conductor's gap (g) as illustrated in the common HF band printed circuit board (PCB) antenna structure in Figure 3(b). C_a is the parasitic capacitance of the antenna, which exists between the coils. In designing the NFC tag antenna, it is crucial to minimize the antenna resistance to reduce heat loss in the antenna. Therefore, the graphene-based NFC tag design must prioritize achieving the lowest possible antenna resistance while maintaining small dimension of the antenna. This effort is essential for minimizing heat loss and enhancing the Q -factor, as the two are directly related, as described in (4).

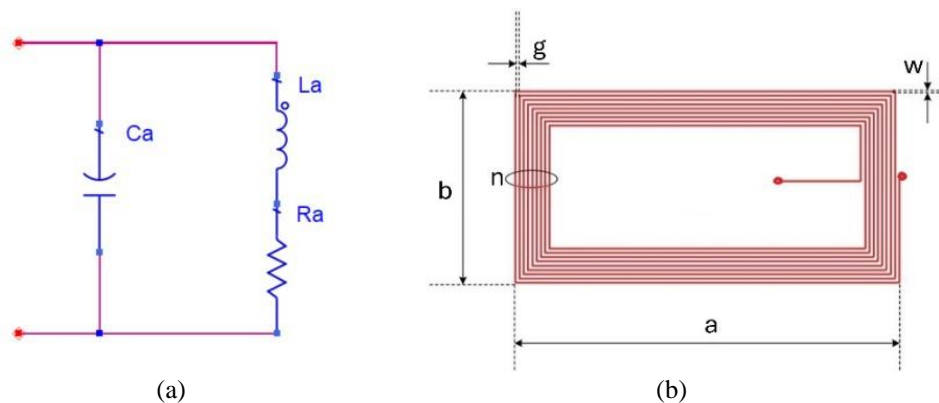


Figure 3. NFC tag antenna: (a) equivalent circuit model and (b) structure

$$Q = \frac{2 \cdot \pi \cdot f_{op} \cdot L}{R} \tag{4}$$

The NFC tag antenna design in Figure 4 was simulated using CST Microwave Studios with different numbers of coil turns, widths and gaps between the coils, in order to achieve the optimum performance. Three antenna designs namely design A, design B, and design C were simulated, as shown in Figures 4(a) to 4(c), respectively. The hybrid graphene conductor was modeled with a conductivity value of 3.95×10^6 S/m, as achieved in section (2.1) and a thickness of $1 \mu\text{m}$. An ISO/IEC 15693 compliant chip from Texas instrument, RF430FRL152HCRGE, with an internal capacitance of 35 pF [29], was integrated at the port of the antenna design. The geometry and simulated values of L_a , R_a , and Q-factor for all designs are summarized in Table 1. The L_a and R_a values were measured at 1 MHz, as recommended in [30], to neglect the capacitive part of the coil antenna, while the Q-factor was measured at 13.56 MHz. Among the three designs, design A and design B have similar Q-factor values, both of which are twice as high as design C. This is due to the wider coil width of design A and design B compared to design C, which reduces the antenna resistance and increases the cross-sectional area for current to flow. Since resistance is inversely proportional to the Q-factor as referred to (4), reducing the antenna resistance contributes to an increase in the antenna's Q-factor. However, compared to design B, design A has 20% smaller dimensions, making it more suitable for placement on various items and surfaces without being overly bulky. Therefore, design A was chosen as the most optimum design for printing and further analysis.

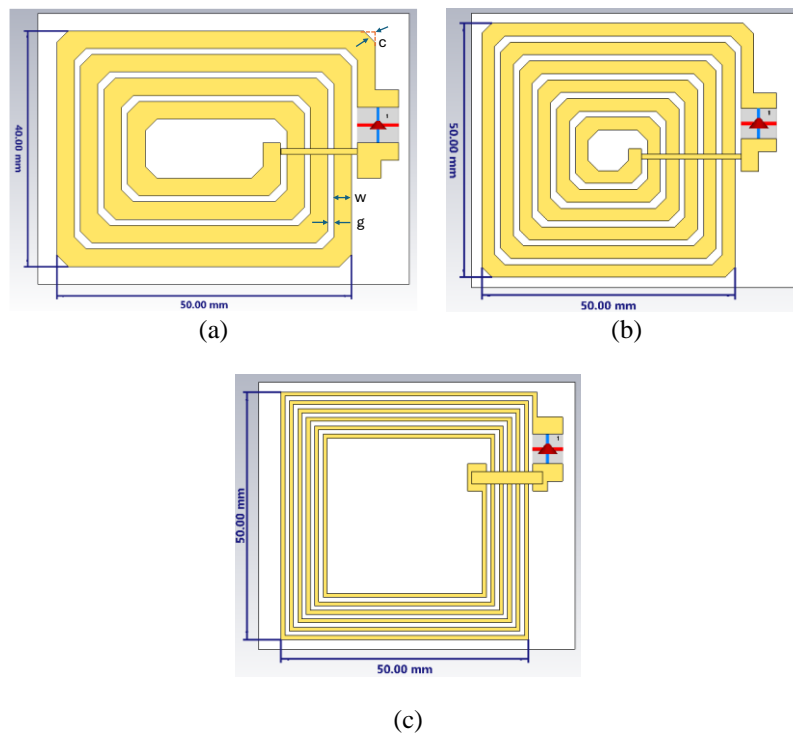


Figure 4. Structure of antenna design for (a) design A, (b) design B, and (c) design C

Table 1. Antenna geometries and simulated L_a , R_a , and Q-factor values

Design	A	B	C
Dimension	50×40	50×50	50×50
Conductor width, w (mm)	3	2.5	0.8
Gap between coils, g (mm)	1	1.2	0.9
Number of turns, n	4	6	6
Chamfer width, c (mm)	2	2	0
L_a (μH) @1 MHz	0.75	1.21	2.35
R_a (Ω) @1 MHz	37.03	65.96	308.77
Q-factor @13.56 MHz	1.2	1.2	0.62

2.3. Fabrication of graphene-based NFC tag antenna

Figure 5 illustrates the fabrication process of the graphene-based NFC tag antenna. The tag antenna was fabricated using inkjet printing technology with the PiXDRO LP50 (SuSS MicroTec). The temperature of the platen can be adjusted between 28 °C to 60 °C. To prevent the ink from spreading, the platen

temperature in this fabrication was set at 40 °C. The antenna was printed with a minimum thickness of 1 μm to reduce the printing difficulty. To ensure flexibility, the graphene conductive material was printed on a PET substrate with an electrical permittivity of 3 and a thickness of 0.12 mm. After printing, the antenna was cured at 40 °C for 30 minutes. The antenna coil and bridge were printed separately and subsequently bonded using silver conductive epoxy, Chemtronics CW2400. The conductive epoxy requires curing at room temperature (25 °C) for 4 hours, with maximum bond strength achieved after 24 hours.

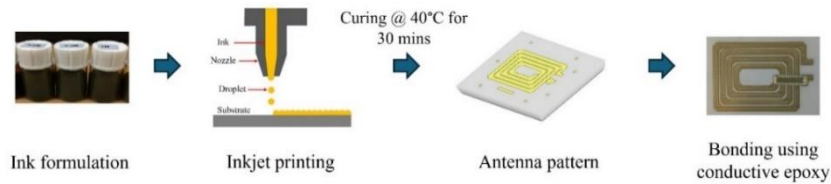


Figure 5. Fabrication process of graphene-based NFC tag antenna

3. RESULTS AND DISCUSSION

This section discusses the simulated and measured results of the proposed NFC tag antenna, including antenna inductance, antenna DC resistance, tag reading range, bending and sensitivity on different surface materials to validate the feasibility of using hybrid graphene-based material as the conductive element for the NFC tag antenna. The hybrid graphene-based NFC tag antenna also has been integrated with the flexible temperature sensor circuit, printed using the same material, and the reliability of the tag for temperature monitoring applications has been evaluated.

3.1. Antenna inductance, L_a and antenna DC resistance, R_a

Figure 6 illustrates the measurement of the electrical properties, including L_a and R_a , of the printed Design A tag antenna to validate the simulation results presented in Table 1. Three samples of the Design A antenna, shown in Figure 6(a), were used to measure L_a and R_a with a Keysight N5232B PNA-L Vector Network Analyzer (VNA), as depicted in Figure 6(b). From the smith chart result, the L_a and R_a values were evaluated at 1 MHz as shown in Figure 6(c), while the Q-factor values were calculated from the network impedance obtained at the operating frequency of 13.56 MHz using (4). The measured results are compared with the CST simulation as presented in Table 2. On average, the simulated and measured results exhibit good agreement with very slight difference for L_a , R_a , and Q-factor values. These findings demonstrate that the graphene-based conductive material is well printed and compatible with the flexible PET substrate, maintaining consistent conductivity throughout the entire coil design, similar to the simulation conditions.

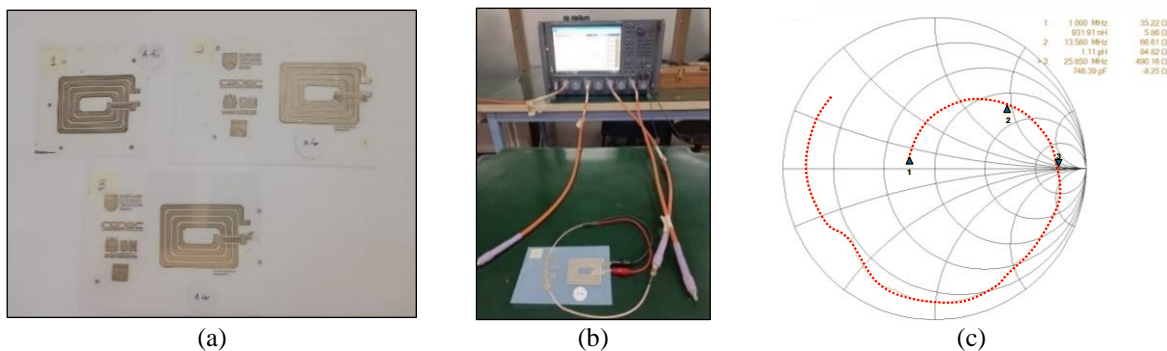


Figure 6. Design A tag antenna's (a) prototypes, (b) measurement setup for antenna inductance and resistance using the Keysight N5232B PNA-L VNA, and (c) example of a Smith chart result

Table 2. Simulated and measured results for design A antenna inductance, resistance, and Q-factor

Parameter	CST simulation	VNA measurements			
		1	2	3	Average
L_a (μH) @1 MHz	0.75	0.88	0.92	0.91	0.90
R_a (Ω) @1 MHz	37.03	50.15	30.96	37.11	39.41
Q-factor @ 13.56 MHz	1.20	0.97	1.67	1.35	1.33

3.2. Tag reading range

The tag reading range in Figure 7 is defined as the maximum distance at which the reader can detect the tag. The tag reading range is determined in the simulation from the magnetic field strength curve, as shown in Figure 7(a). The distance at 1.5 A/m is considered the maximum reading distance, as 1.5 A/m is the standard value for the minimum field strength required to activate the chip [31]. According to the graph, the proposed graphene-based tag antenna achieves a maximum reading range of approximately 3.2 cm.

The graph in Figure 7(b) illustrates the relationship between the tag reading range and the antenna resonance frequency as a function of the tuning capacitance value. Without any tuning, the tag can already be detected with a reading range of up to 1.8 cm. Increasing the tuning capacitance to 75 pF maximizes the tag reading range at a resonant frequency of 15 MHz, with a distance of approximately 3 cm. However, as the tuning capacitance increases higher, the resonant frequency shifts to a lower frequency and the reading range decreases. The minimum distance achieved is 1.3 cm with a tuning capacitance value of 200 pF and a resonance frequency of 11.53 MHz. Below this frequency, the tag antenna cannot be detected as the resonant frequency does not match the reader, resulting in no magnetic coupling. The maximum measured reading range shows very close agreement to the simulation and it is within the typical detection range for a smartphone, which is between 1 and 5 cm [32].

Figure 8 is measurement setup. The simulated tag reading range was then verified through measurement using the experimental setup shown in Figure 8(a). In this setup, the antenna was connected in parallel with the tuning capacitance C_{tun} on the breadboard and the RF430FRL152HEVM board from Texas Instruments, which includes RF430FRL152H chip. To detect the tag and measure the reading range, an NFC-enabled smartphone, specifically the Xiaomi 11T, was employed, and the distance between the tag and the smartphone was measured using a vernier calliper. The tuning capacitance was varied from 50 pF to 200 pF to determine the highest reading range achievable by the antenna. The resonance frequency was observed using the VNA, as depicted in Figure 8(b), where the tag antenna is brought closer to a coil antenna with a resonant frequency of over 50 MHz connected to the VNA.

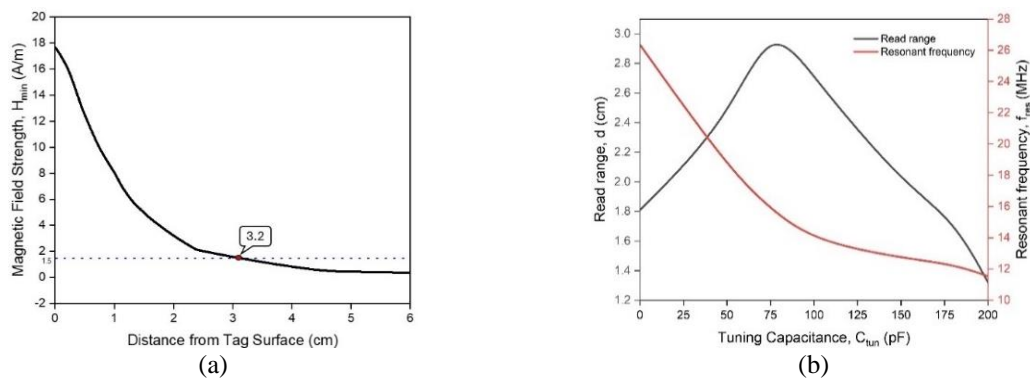


Figure 7. Reading range observation through (a) magnetic field strength as a function of distance from tag surface (z-axis) and (b) measured tag reading range with respective resonant frequency and tuning capacitance value

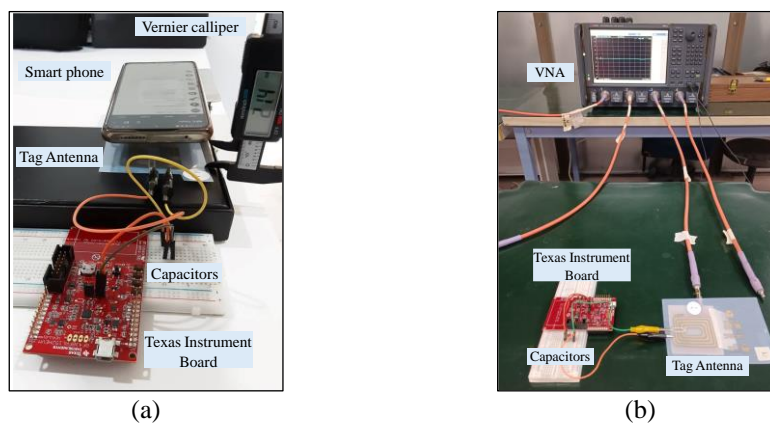


Figure 8. Measurement setup for (a) tag reading range and (b) antenna resonant frequency

3.3. Effect of bending at different radius

The flexibility of the graphene-based tag antenna has also been assessed by varying the bending radius. In the simulation shown in Figure 9, the antenna is bent on a cylindrical foam with ϵ_r of 1, at different angles by varying the cylindrical bending radius, r , within the 1.5 cm to 4.5 cm range. The relationship between the bending radius and angle can be determined using the arc length, S formula in (5), where the bending angle, θ is inversely proportional to the radius of the cylinder, r . Thus, an increase in radius (1.5 cm to 4.5 cm) results in a decrease in the bending angle (190.9° to 63.7°). The simulated results of the S-parameter for various bending radius are shown in Figure 9(a). The result indicates that the antenna resonant frequency shifts to a higher frequency by less than 1 MHz for the maximum bending angle. This shift is insignificant and remains within the acceptable operating frequency range for NFC tag ($13.56 \text{ MHz} < f_{\text{Tag}} < 16 \text{ MHz}$) [33]. The frequency shift is attributed to the decrease in antenna inductance, L_a , as illustrated in Figure 9(b). However, bending may contribute to a decrease in coupling efficiency with the reader, as the magnetic field intensity is reduced with an increase in the bending angle, as shown in Figure 9(c). The increase in the bending angle leads to an asymmetrical distribution of the magnetic field due to the distortion of the current flow and magnetic field patterns within the antenna structure.

$$S = \theta \cdot R \approx \frac{S}{R} = \theta \quad (5)$$

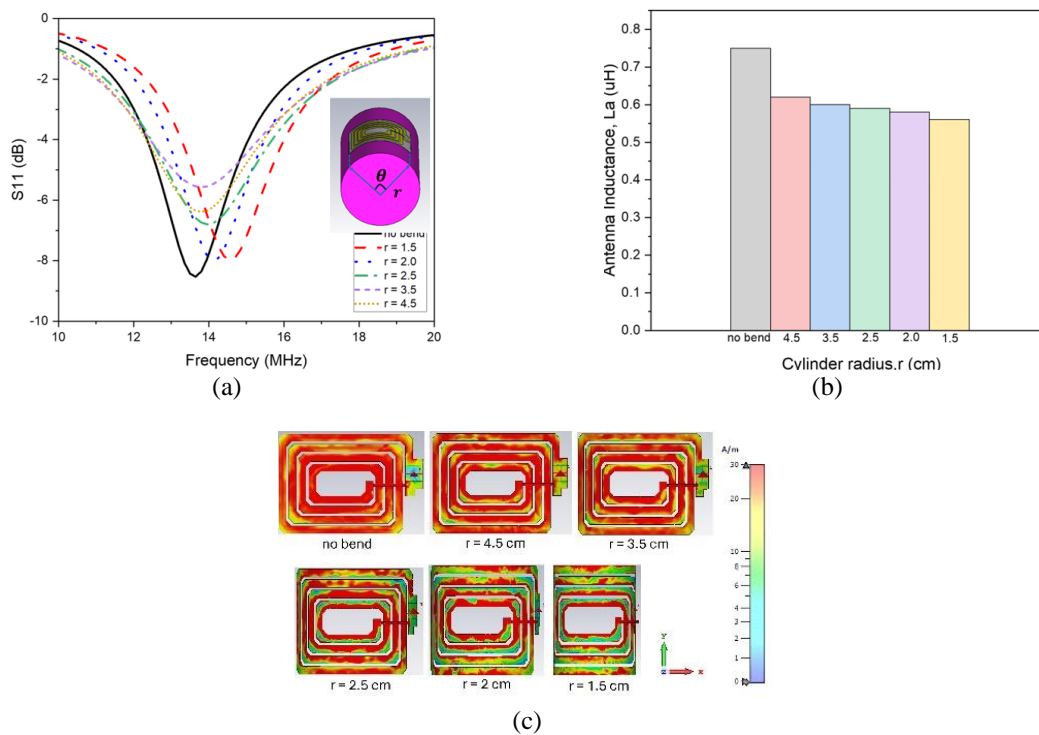


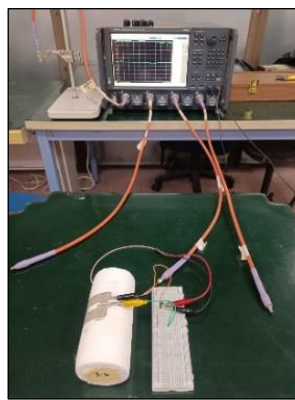
Figure 9. Simulation results of (a) S-parameter, S_{11} ; (b) antenna inductance, L_a ; and (c) magnetic field distribution with the variation of cylinder radius, r

The measurement at different bending angles, as depicted in Figure 10, were conducted to verify the simulated results. The tag antenna was attached to different sizes of cylinder foam, as shown in Figure 10(a). The tag reading range was measured, and the shift of antenna's resonant frequency from the operating frequency of 13.56 MHz was observed using VNA, as shown in Figure 10(b). The results in Figure 11 indicate that the antenna's resonant frequency remains relatively constant across various surface bending of cylinder foams, except for the cylinder foam with $r=1.5 \text{ cm}$ ($\theta=190.9^\circ$), which shows a slight shift of around 1 MHz to a higher frequency, as illustrated in Figure 11(a). Although the resonant frequency is not significantly affected by the bending, the tag reading range decreases from 2.4 cm to 1.3 cm as the bending angle is increased from 63.7° to 190.9° , which is equal to the decrease of cylinder radius from 4.5 cm to 1.5 cm, as depicted in Figure 11(b). This occurs because the bending angle is more significant when the cylinder radius is smaller, reducing the antenna's accessible surface area for the reader. Since the surface area is

directly proportional to the induced magnetic field, the smaller the surface area, the less magnetic field is induced in the tag antenna, thereby reducing the tag reading range. These results prove that the proposed tag antenna is robust to curvature, with the smallest detection range achieved being 1.3 cm.



(a)



(b)

Figure 10. Measurement at different bending angle using (a) cylinder foams with varying radius and (b) measurement setup for antenna resonant frequency using VNA

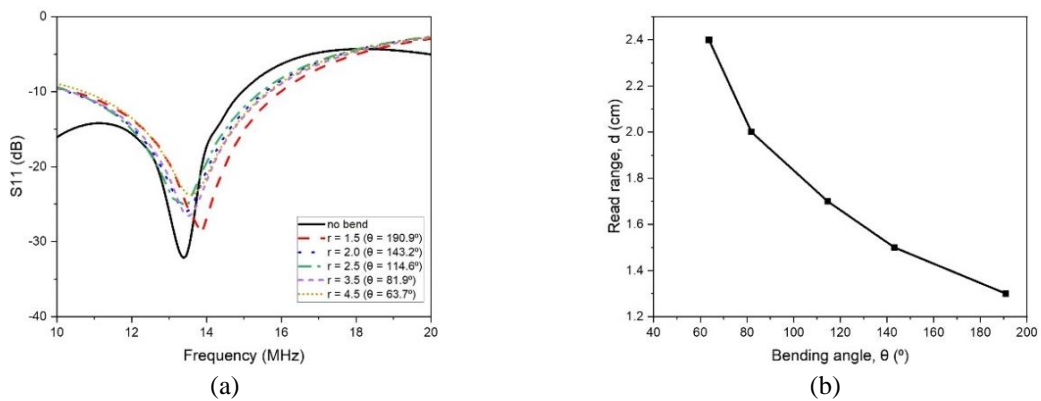


Figure 11. Measurement results of (a) S-parameter, S₁₁ and (b) reading range with variation of bending angle

3.4. Sensitivity on different surface

The sensitivity of the graphene-based tag when attached to different materials, as depicted in Figure 12, was evaluated. The tag antenna was affixed to various materials, including plastic, carton box, wood, and metal, as shown in Figures 12(a)-(d), respectively, respectively. According to the measurements, the performance of the tag antenna is not much affected by plastic, carton boxes, or wood materials, where the antenna resonant frequency remain relatively constant when attached to these materials, with only slight shift

of approximately 1 MHz from the antenna in free air, as depicted in Figure 13. However, when the tag antenna is mounted to metal, it loses performance and does not resonate at the required operating frequencies. This behaviour is due to the presence of an eddy current on the metallic component, which generate a magnetic field in the opposite direction, weakening the field of the NFC reader. To lessen the influence of eddy current on the tag antenna, a magnetic sheet such as ferrite or amorphous can be attached to the back of the tag antenna, as recommended in [34], [35].

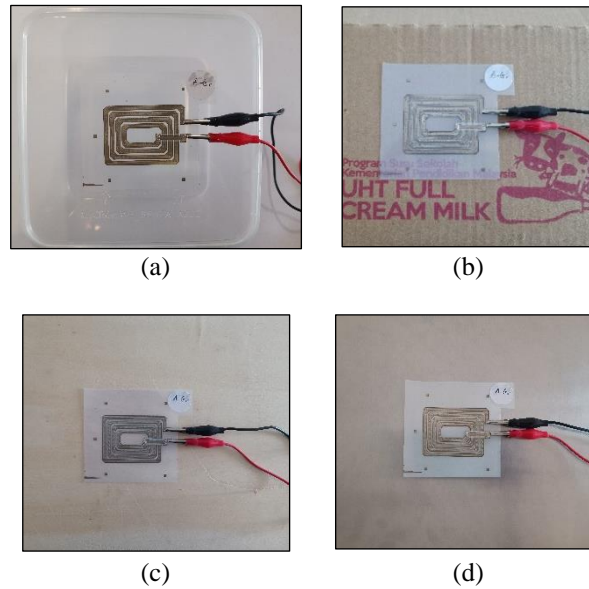


Figure 12. Antenna attached to different materials: (a) plastic, (b) carton box, (c) wood, and (d) metal

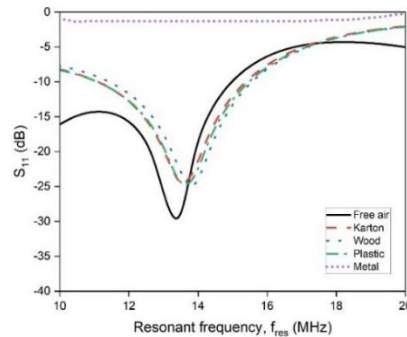


Figure 13. Measurement results of S_{11} when different materials are attached to the tag

3.5. Integration with temperature sensor

For the temperature monitoring application, the proposed graphene-based tag antenna in Figure 14 is integrated with a flexible temperature circuit comprising the RF430FRL152H chip and 100 k Ω NTC thermistor from Sunlord, which serves as the temperature sensor. Figure 14(a) illustrates the prototype of the tag antenna with the integrated circuit. The tag antenna and the temperature circuit are printed using the proposed graphene-based conductive material. Surface-mount device (SMD) components, including resistors and capacitors, are mounted on the circuit using silver conductive epoxy, Chemtronics CW2400, with the aid of a stencil. Figure 14(b) depicts the schematic circuit diagram of the tag for temperature monitoring application. The designed antenna is connected to pin 1 and 2 of the chip. Meanwhile, the temperature sensor (RT1) is connected to the ADC2 pin and grounded to the virtual ground of the sensor reference potential (SVSS). A reference resistor (R_{ref}), with the same value as the thermistor (100 k Ω), is connected to ADC1 and SVSS to achieve more accurate temperature measurement. The general equation of the temperature change of a thermistor in (6) is utilized to calculate the measured temperature in relation to the resistance of

the thermistor [36]. Here, R_t represents the resistance value at temperature T , R_0 denotes the reference resistance value at the reference temperature T_0 and β represents the material coefficient of the thermistor.

$$R_t = R_0 e^{\left(\frac{\beta}{T} - \frac{\beta}{T_0}\right)} \tag{6}$$

Figure 15 illustrates the temperature monitoring of the proposed graphene-based tag integrated with the temperature sensor. The temperature was wirelessly monitored using a Xiaomi 11T smartphone with an NFC temperature monitoring app, as depicted in the measurement setup shown in Figure 15(a). The temperature was varied by adjusting the distance of the blower from the tag antenna, and the app's temperature readings were compared with the actual controlled temperature. The temperature monitoring app has been enhanced from the previously developed app by Texas instruments to make it suitable for graphene-based tag antenna as illustrated in Figure 15(b). The previous app was only applicable for metal-based tag antennas, providing accurate temperature measurements exclusively for such antennas. However, when this app is used for a graphene-based tag antenna, the measured temperature significantly increases compared to the real controlled temperature, as illustrated in the first correlation of Figure 15(c). This discrepancy arises due to the higher resistance of graphene material compared to metallic material, affecting the voltage present at the input of the ADC2.

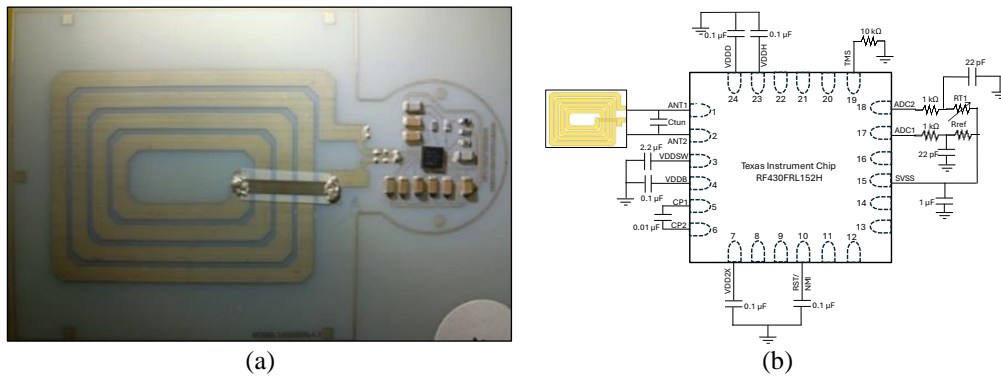


Figure 14. Graphene-based tag antenna with temperature sensor: (a) prototype and (b) schematic circuit diagram

To overcome this issue, a two-step linear regression was performed between the actual temperature and the temperature measured using the app, as shown in Figure 15(c). The first linear regression involves comparing the real temperature with the app temperature using the original app, whereas the second linear regression involves correlating the real temperature with the app temperature using the measured values from the first regression. The linear fit equations for the first and second regressions are given in (7) and (8), respectively. Both equations are incorporated into the app coding in Android Studio, and the final results of applying both equations are presented in Figure 15(c). The temperature difference between real and app temperatures is within ± 2 °C, making it suitable for temperature monitoring applications.

$$App\ Temp = 0.98133 (Real\ temp) + 21.20369 \tag{7}$$

$$App\ Temp = 0.93243 (Real\ temp) + 2.84593 \tag{8}$$

The comparison of the proposed tag with recently published graphene-based NFC tags is shown in Table 3. The proposed conductive material, hybrid graphene-silver, exhibits the highest conductivity value compared to other graphene-based materials from previous work. Despite its lower printed thickness of 1 μm , the proposed tag achieves performance comparable to other graphene-based NFC tags, particularly in terms of read range and application. Although its reading range is lower than that of [8], it still meets the required range for an NFC tag when detected by a smartphone, typically between 1 cm and 5 cm [32]. The low thickness of printed graphene-based conductive materials also offers advantages in terms of flexibility, lightweight design, and ease of printing for the NFC tag. Regarding size, most tags from previous work are bulkier than the proposed tag, which may limit their attachment to certain items. Additionally, the integration of the tag antenna with a flexible temperature monitoring circuit makes it suitable for attachment to conformal structures, unlike the tags in [21] and [37], which have sensor circuits mounted on PCB substrates,

reducing their flexibility. Meanwhile, the tags presented in [20] and [8] only integrate with the NFC chip without any available sensors.

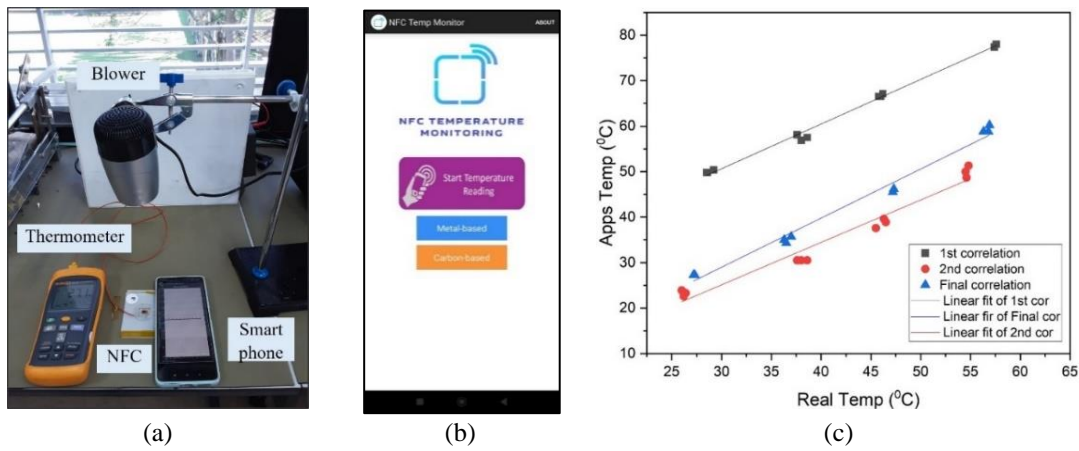


Figure 15. Temperature monitoring: (a) measurement setup, (b) enhanced temperature monitoring app, and (c) correlation between app temperature and real temperature with linear regressions analysis

Table 3. Comparison of the graphene-based NFC tag antenna with the proposed tag

Ref	Material (substrate)	Conductivity (s/m)/thickness	Ant size (mm ²)	Read range (cm)	Reader	Reader spec (output power)	NFC chip (min input power)	Application	Integrate circuit/sensor
This work	Hybrid graphene silver (PET)	$3.95 \times 10^6 / 1 \mu\text{m}$	50x40	3	Smartphone Xiaomi 11T	20 dBm - 23 dBm (100 mW-200 mW)	RF430FRL152H Texas instrument (2.85 mW)	Temp monitoring	Yes (flex)
[20]	Stacked graphene multilayer (G-paper) (PET, PEN, PC, PVC, paper & silk)	$4.2 \times 10^5 / 55 \mu\text{m}$	75x45	Few cm	ST Micro CR95HF	55 mW - 230mW	NXP ICODE SL2S2002 (40 μW)	Smartcard, wearable bracelet	No
[8]	GO-assembled films (PET)	$\sim 10^6 / 25 \mu\text{m}$	80x50	7.5	Voyantic tagformance	-10 dBm to 25 dBm (10 mW to 316 mW)	NXP ICODE SL2S2602 (40 μW)	Wearable bracelet, smart card	No
[21]	Graphene flakes (paper)	$3.33 \times 10^5 / \text{NA}$	74x53	-	Texas instrument TRF7970A EVM	20 dBm - 23 dBm (100 mW-200 mW)	RF430FRL152H Texas instrument (2.85 mW)	Photosensor	Yes (PCB)
[37]	Graphene laminate (graphene nano flakes)	$3.7 \times 10^4 / 7.8 \mu\text{m}$	65x55	2.5	Texas instrument TRF7970A EVM	20 dBm - 23 dBm (100 mW-200 mW)	RF430FRL152H Texas instrument (2.85 mW)	Temp Monitoring	Yes (PCB)

4. CONCLUSION

This paper has successfully validated the feasibility of using the proposed hybrid graphene-based conductive materials, composed of rGO and silver nanoparticles, in flexible NFC tags. The design A tag antenna, inkjet-printed using the proposed material, demonstrated a maximum reading range of up to 3 cm. The tag antenna was also verified to be robust and flexible, withstanding bending at various angles without significant performance degradation. It remained detectable at a maximum range of up to 1.3 cm at a 190.9° ($r=1.5$ cm) bending angle. Additionally, the tag showed consistent performance when attached to various surfaces, including plastic, carton and wood, except for metal surfaces due to the presence of eddy currents. Integrating the tag antenna with the flexible temperature circuit also produced reliable temperature readings, with the difference between the actual and app-recorded temperatures being minimal, within ± 2 °C. For future studies, the proposed tag antenna could be applied to real-world food quality monitoring across different temperature ranges, where both real-time data and material robustness are crucial. Additionally, alternative substrates, such as thermoplastic polyurethane (TPU), which offer stretchability, could be explored for use with the hybrid graphene-based material to improve the durability and flexibility of the tag.

ACKNOWLEDGEMENTS

The author would like to convey the deepest gratitude to the Universiti Teknologi MARA, Cawangan Pulau Pinang, the Antenna Research Center (ARC), the Collaborative Microelectronic Design Excellence Centre (CEDEC) USM and MIMOS Berhad for support and guidance. This project was supported by Strategic Research Fund (SRF) under Ministry of Science, Technology, and Innovation (MOSTI) with Fund Code: SF 202000 PG2P2 Printed Hybrid Electronics of Electric and Autonomous Vehicle.




REFERENCES

- [1] F. Bibi, C. Guillaume, N. Gontard, and B. Sorli, "A review: RFID technology having sensing aptitudes for food industry and their contribution to tracking and monitoring of food products," *Trends in Food Science & Technology*, vol. 62, pp. 91–103, Apr. 2017, doi: 10.1016/J.TIFS.2017.01.013.
- [2] F. Requena, N. Barbot, D. Kaddour, and E. Perret, "Combined temperature and humidity chipless RFID sensor," *IEEE Sensors Journal*, vol. 22, no. 16, pp. 16098–16110, Aug. 2022, doi: 10.1109/JSEN.2022.3189845.
- [3] M. C. Caccami, M. Y. S. Mulla, C. Occhiuzzi, C. Di Natale, and G. Marrocco, "Design and experimentation of a batteryless on-skin RFID graphene-oxide sensor for the monitoring and discrimination of breath anomalies," *IEEE Sensors Journal*, vol. 18, no. 21, pp. 8893–8901, Nov. 2018, doi: 10.1109/JSEN.2018.2867208.
- [4] C. A. Tucker, U. Muehlmann, and M. Gebhart, "Contactless power transmission for NFC antennas in credit-card size format," *IET Circuits, Devices and Systems*, vol. 11, no. 1, pp. 95–101, Jan. 2017, doi: 10.1049/iet-cds.2015.0023.
- [5] P. Sittithai, K. Phaebua, T. Lertwiriyaprapa, and P. Akkarakthalin, "Magnetic field shaping technique for HF-RFID and NFC systems," *Radioengineering*, vol. 27, no. 1, pp. 121–128, 2019, doi: 10.13164/RE.2019.0121.
- [6] M. Boada, A. Lazaro, R. Villarino, E. Gil-Dolcet, and D. Girbau, "Battery-less NFC bicycle tire pressure sensor based on a force-sensing resistor," *IEEE Access*, vol. 9, pp. 103975–103987, 2021, doi: 10.1109/ACCESS.2021.3099946.
- [7] A. Lazaro, M. Boada, R. Villarino, and D. Girbau, "Battery-Less Smart Diaper Based on NFC Technology," *IEEE Sensors Journal*, vol. 19, no. 22, pp. 10848–10858, 2019, doi: 10.1109/JSEN.2019.2933289.
- [8] S. Li and R. Song, "Wearable near-field communication bracelet based on highly conductive graphene-assembled films," *International Journal of RF and Microwave Computer Aided Engineering*, no. July 2020, 2020, doi: 10.1002/mmce.22479.
- [9] I. Ortego, N. Sanchez, J. Garcia, F. Casado, D. Valderas, and J. I. Sancho, "Inkjet printed planar coil antenna analysis for NFC technology applications," *International Journal of Antennas and Propagation*, vol. 2012, 2012, doi: 10.1155/2012/486565.
- [10] W. Pachler *et al.*, "A silver inkjet printed ferrite NFC antenna," in 2014 *Loughborough Antennas and Propagation Conference (LAPC)*, IEEE, Nov. 2014, pp. 95–99. doi: 10.1109/LAPC.2014.6996329.
- [11] L. Hakola *et al.*, "Sustainable roll-to-roll manufactured multi-layer smart label," *The International Journal of Advanced Manufacturing Technology*, vol. 117, no. 9–10, pp. 2921–2934, Dec. 2021, doi: 10.1007/s00170-021-07640-z.
- [12] A. Lamminen *et al.*, "Graphene-flakes printed wideband elliptical dipole antenna for low-cost wireless communications applications," *IEEE Antennas and Wireless Propagation Letters*, vol. 16, no. March, pp. 1883–1886, 2017, doi: 10.1109/LAWP.2017.2684907.
- [13] Y. Z. N. Htwe and M. Mariatti, "Printed graphene and hybrid conductive inks for flexible, stretchable, and wearable electronics: progress, opportunities, and challenges," *Journal of Science: Advanced Materials and Devices*, vol. 7, no. 2, p. 100435, 2022, doi: 10.1016/j.jsamd.2022.100435.
- [14] R. H. Abd and H. A. Abdulnabi, "Design of graphene-based multi-input multi-output antenna for 6G/IoT applications," *Indonesian Journal of Electrical Engineering and Computer Science (IJECS)*, vol. 31, no. 1, pp. 212–221, Jul. 2023, doi: 10.11591/ijeecs.v31.i1.pp212-221.
- [15] M. Zolfaghari-Koochi and M. Neshat, "Antenna efficiency in graphene-based THz photoconductive antennas," *22nd Iranian Conference on Electrical Engineering, ICEE 2014*, no. Icee, pp. 1587–1590, 2014, doi: 10.1109/IranianCEE.2014.6999789.
- [16] M. Tamagnone, J. S. Gómez-Díaz, J. R. Mosig, and J. Perruisseau-Carrier, "Analysis and design of terahertz antennas based on plasmonic resonant graphene sheets," *Journal of Applied Physics*, vol. 112, no. 11, 2012, doi: 10.1063/1.4768840.
- [17] P. Kopyt *et al.*, "Graphene-based dipole antenna for a UHF RFID tag," *IEEE Transactions on Antennas and Propagation*, vol. 64, no. 7, pp. 2862–2868, 2016, doi: 10.1109/TAP.2016.2565696.
- [18] X. Huang, T. Leng, X. Zhang, J. C. Chen, and K. H. Chang, "Binder-free highly conductive graphene laminate for low cost printed radio frequency applications," *Applied Physics Letters*, vol. 203105, no. May, pp. 19–23, 2015, doi: 10.1063/1.4919935.
- [19] M. Akbari, M. W. A. Khan, M. Hasani, T. Bjorninen, L. Sydanheimo, and L. Ukkonen, "Fabrication and characterization of graphene antenna for low-cost and environmentally friendly RFID tags," *IEEE Antennas and Wireless Propagation Letters*, vol. 15, pp. 1569–1572, 2016, doi: 10.1109/LAWP.2015.2498944.




- [20] A. Scidà *et al.*, “Application of graphene-based flexible antennas in consumer electronic devices,” *Materials Today*, vol. 21, no. 3, pp. 223–230, 2018, doi: 10.1016/j.mattod.2018.01.007.
- [21] T. Leng *et al.*, “Printed graphene/WS2 battery-free wireless photosensor on papers,” *2D Materials*, vol. 7, no. 2, 2020, doi: 10.1088/2053-1583/ab602f.
- [22] E. B. Secor, P. L. Prabhuramirashi, K. Puntambekar, M. L. Geier, and M. C. Hersam, “Inkjet printing of high conductivity, flexible graphene patterns,” *Journal of Physical Chemistry Letters*, vol. 4, no. 8, pp. 1347–1351, Apr. 2013, doi: 10.1021/jz400644c.
- [23] X. Huang, T. Leng, M. Zhu, X. Zhang, J. Chen, and K. Chang, “Highly flexible and conductive printed graphene for wireless wearable communications applications,” *Nature Publishing Group*, no. July, pp. 1–8, 2015, doi: 10.1038/srep18298.
- [24] T. Leng, X. Huang, K. Chang, J. Chen, M. A. Abdalla, and Z. Hu, “Graphene nanoflakes printed flexible meandered-line dipole antenna on paper substrate for low-cost RFID and sensing applications,” *IEEE Antennas and Wireless Propagation Letters*, vol. 15, no. c, pp. 1565–1568, 2016, doi: 10.1109/LAWP.2016.2518746.
- [25] H. Chen *et al.*, “Advances in graphene-based flexible and wearable strain sensors,” *Chemical Engineering Journal*, vol. 464, p. 142576, May 2023, doi: 10.1016/j.cej.2023.142576.
- [26] N. Abdul Rashid, N. D. S. Zambri, A. S. Abd Aziz, M. H. S. Mohd Jaafar, and S. Sulaiman, “Characterization of hybrid reduced graphene oxide - silver nanoparticles conductive ink for flexible electronics applications,” in *Proceedings of the 4th International Symposium on Advanced Materials and Nanotechnology 2020, (i-SAMN2020)*, 2020.
- [27] A. Nag *et al.*, “Graphene-based wearable temperature sensors: a review,” *Materials & Design*, vol. 221, p. 110971, Sep. 2022, doi: 10.1016/j.matdes.2022.110971.
- [28] NH. Instruments, “Resistivity measuring systems NH Instruments,” 2022. [Online]. Available: <https://www.nh-instruments.de/wp-content/uploads/NH-Instruments-Resistivity-Meters-Small.pdf>
- [29] Texas Instruments, “RF430FRL15xH firmware user’s guide,” Texas Instruments, no. December, pp. 1–57, 2014, [Online]. Available: <http://www.ti.com/lit/ug/slau603b/slau603b.pdf>
- [30] J. Q. Zhu, Y. L. Ban, C. Y. D. Sim, and G. Wu, “NFC antenna with nonuniform meandering line and partial coverage ferrite sheet for metal cover smartphone applications,” *IEEE Transactions on Antennas and Propagation*, vol. 65, no. 6, pp. 2827–2835, 2017, doi: 10.1109/TAP.2017.2690532.
- [31] J. Victoria, A. Suarez, P. A. Martinez, A. Alcarria, A. Gerfer, and J. Torres, “Improving the Efficiency of NFC Systems through Optimizing the Sintered Ferrite Sheet Thickness Selection,” *IEEE Transactions on Electromagnetic Compatibility*, vol. 62, no. 4, pp. 1504–1514, Aug. 2020, doi: 10.1109/TEMC.2020.3003800.
- [32] P. Escobedo *et al.*, “Smart facemask for wireless CO2 monitoring,” *Nature Communications*, vol. 13, no. 1, pp. 1–12, Jan. 2022, doi: 10.1038/s41467-021-27733-3.
- [33] J. Grosinger, “Robustly operating: passive near-field communication systems in metal environments,” *IEEE Microwave Magazine*, vol. 24, no. 4, pp. 30–39, Apr. 2023, doi: 10.1109/MMM.2022.3233508.
- [34] M. Benavides, D. Miralles, A. Andújar, and J. Anguera, “Effects on human body and conductive body over a near field communication antenna,” *Journal of Electromagnetic Waves and Applications*, vol. 35, no. 9, pp. 1235–1246, 2021, doi: 10.1080/09205071.2021.1875889.
- [35] N. M. Faudzi *et al.*, “Comparative study of ferrite and amorphous shielding materials for NFC tag antenna on metal,” in *2023 IEEE International Symposium on Antennas and Propagation (ISAP)*, IEEE, Oct. 2023, pp. 1–2. doi: 10.1109/ISAP57493.2023.10388437.
- [36] J. Liu, Y. Wang, X. Li, J. Wang, and Y. Zhao, “Graphene-based wearable temperature sensors: a review,” *Nanomaterials*, vol. 13, no. 16, p. 2339, Aug. 2023, doi: 10.3390/nano13162339.
- [37] K. Pan *et al.*, “Sustainable production of highly conductive multilayer graphene ink for wireless connectivity and IoT applications,” *Nature Communications*, vol. 9, no. 1, p. 5197, Dec. 2018, doi: 10.1038/s41467-018-07632-w.

BIOGRAPHIES OF AUTHORS






Najwa Mohd Faudzi    received her B.Sc. degree in Electrical Engineering from Hochschule Osnabrueck, Germany in 2012 and M.Sc. degree in Electrical Engineering from Universiti Teknologi MARA (UiTM) Shah Alam, Malaysia in 2015. Currently, she is pursuing Ph.D. degree in Electrical Engineering, Universiti Teknologi MARA Cawangan Pulau Pinang, Malaysia. Her research interests include RFID systems, near-field communication, antenna designs, microwave technologies, wearable and flexible antennas. She can be contacted at email: najwa_nmf@yahoo.com.






Ahmad Rashidy Razali    received his B.Eng (Hons) degree in Electronic Engineering from University Tenaga Nasional, Malaysia in 2002, M.Sc. degree in Mobile and Satellite Communication Engineering from University of Surrey, United Kingdom in 2004. In 2012, he received his Ph.D. in Telecommunication Engineering from University of Queensland, Australia. He is currently a Professor at University Technology Mara, Pulau Pinang Malaysia. He is a professional engineer recognized by Board of Engineer Malaysia (BEM). His research interests include in antenna, microwave, and communication system. He can be contacted at email: ahmad370@gmail.com.com.






Asrulnizam Abd. Manaf    received the B.Eng. Degree and M.Sc. degree in Electrical and Electronic Engineering from Toyohashi University of Technology (TUT), Japan in 2001 and 2005 respectively. He received the Ph.D. degree in Fundamental of Sciences and Technology from Keio University, Japan in 2009. His professorial interests include the areas of integration fluidic-based Bio/Physical MEMS sensor with CMOS readout circuitry, micro fluidic based inductor, micro fluidic based memristor, micro 3D fabrication and silicon micromachining technology, flexible micro thermo electric generator (mTEG), flexible ultra thin film, graphene based electronic devices and IoT devices. He can be contacted at email: eeasrulnizam@usm.my.






Nurul Huda Abd Rahman    received the M.Eng. degree in electronic from the University of Surrey, Guildford, U.K., in 2008, and the Ph.D. degree in electric, electronic and systems engineering from the Universiti Kebangsaan Malaysia, in 2014. She joined Astronautic Technology (M) Sdn. Bhd., as a Spacecraft Engineer, in 2008, where she was involved in various small-class satellite development and research and development projects. In 2014, she was appointed as a Senior Lecturer with the Universiti Teknologi MARA Malaysia (UiTM). She is currently working with UiTM. Her current research interests include antennas for space and terrestrial applications, array antennas, reflector and lens antennas, wearable and flexible antennas, RF and microwave design, and electromagnetic analysis. She has been the professional engineer of the Board of Engineers Malaysia (BEM), since 2019. She can be contacted at email: nurulhuda0340@uitm.edu.my.






Ahmad Azlan Ab Aziz    is an accomplished academician with a doctorate in Electrical and Electronic Engineering and years of experience as an assistant professor at Universiti Teknologi Brunei (UTB). With antenna design and military communication expertise, the author is recognized as a professional engineer and ASEAN chartered professional engineer (ACPE) in electrical engineering, making them a top authority in the field. Their insights and ideas are valuable resources for those seeking to better understand communications and military communication. He can be contacted at email: 9m2agc@gmail.com.






Syed Muhammad Hafiz    received his B.Sc. (Physics) degree in 2014 and his Ph.D. in Nanotechnology in 2017, both from the University of Malaya. During his postgraduate studies, he was actively involved in synchrotron facilities located in Thailand and Taiwan, which featured a variety of spectroscopic and microscopy workstations such as X-ray photoelectron spectroscopy (XPS) and low-energy electron microscopy (LEEM). Upon graduation, he successfully established a university start-up company that won the Malaysia Commercialization Year (MCY) 2018 main award in the category of Research Entrepreneur Award, receiving a cheque of RM 130,000. Currently, he is attached to the Advanced Materials and Semiconductor Technology Department at MIMOS Berhad, where he is actively involved in R&D related to automated solution-phase chemical synthesis of graphene-related nanomaterials and pilot-scale fabrication processes for flexible electronic devices using additive manufacturing techniques such as inkjet printing and photonic soldering. He can be contacted at email: syedhafiz27@gmail.com.






Suraya Sulaiman    received her B. Sc degree in Electrical, Electronics and Systems Engineering from Universiti Kebangsaan Malaysia in 2003 and M. Sc degree in Electrical, Electronics and Systems Engineering from Universiti Kebangsaan Malaysia in 2008. Currently, she is working as a researcher in MIMOS Berhad, Malaysia. Her research interest includes printed flexible electronics for displays, sensors and consumer applications, inkjet-printed technology, semiconductor technologies and RFID systems. She can be contacted at email: surayas@ump.edu.my.






Nora'zah Abdul Rashid    received her B.Sc. degree in Applied Chemistry from Universiti Kebangsaan Malaysia in 1994. Currently, she is working as a researcher in MIMOS Berhad, Malaysia. Her current research interest includes the development of advanced materials in printed flexible electronics for displays, sensors and consumer applications, inkjet-printed technology, semiconductor technologies, and RFID systems. She can be contacted at email: norazah@mimos.my.



Amirudin Ibrahim    received his B. Eng degree in Electrical Engineering (Telecommunication) in 2010 and M. Eng in Electrical Engineering from Universiti Teknologi Malaysia (UTM) in 2010 and 2015 respectively. Currently, he is pursuing Ph.D. degree in Electrical Engineering, Universiti Teknologi MARA Cawangan Pulau Pinang, Malaysia. His research interests include antenna design, wearable polymer antenna material, specific absorption rate, and mobile communications. He can be contacted at email: amirudin4854@uitm.edu.my.



Aiza Mahyuni Mozi    received her B. Eng degree in Electrical Engineering from Universiti Malaysia Perlis, Malaysia in 2007 and M. Eng degree in Electrical Engineering from Universiti Tun Hussein Onn Malaysia (UTHM), Malaysia in 2009. Currently, she is pursuing Ph.D. degree in Electrical Engineering, Universiti Teknologi MARA Cawangan Pulau Pinang, Malaysia. Her research interests include antenna sensors, wearable and flexible antennas, and microwave technologies. She can be contacted at email: aiza_mahyuni@ppinang.uitm.edu.my.